引用格式：LIU Yuan, SHEN Xiaoyan, ZHOU Shinan, et al. Micro-angle Measurement Method and Its Accuracy Evaluation Based on Fabry-Perot Etalon[J]. Acta Photonica Sinica, 2021, 50(7):0712004
刘源,沈小燕,周世南,等.基于法布里－珀罗标准具的微小角度测量及不确定度评定方法[J].光子学报,2021,50(7):0712004

基于法布里－珀罗标准具的微小角度测量及不确定度评定方法

刘源[1],沈小燕[1],周世南[1],郭旭波[2],禹静[1],李东升[1],蓝旭辉[1]
(1 中国计量大学 计量测试工程学院,杭州 310018)
(2 清华大学 物理系,北京 100084)

摘　要:研究了一种基于法布里－珀罗标准具多光束干涉成像的微小角度测量方法。通过计算同心干涉圆环圆心位置变化量(圆心位移量)和成像物镜焦距,实现反射镜微小偏转角度的测量。采用相对测量原理,构建了基于圆心位移量不确定度分量和成像物镜焦距不确定度分量的微小角度测量不确定度评定模型。选取2 mm间隔的F-P标准具进行微小角度的测量实验研究,并进行了数据处理。实验结果表明,在600″微小角度测量范围内,测量不确定度不大于0.132″;在40″微小角度测量范围内,测量不确定度不大于0.045″。该方法可为具有自校准特性的、更高准确度的微小角度测量的实现提供参考。

关键词:微小角度测量;法布里－珀罗标准具;高准确度;不确定度评定;测量方法
中图分类号:O436　　**文献标识码**:A　　**doi**:10.3788/gzxb20215007.0712004

Micro-angle Measurement Method and Its Accuracy Evaluation Based on Fabry-Perot Etalon

LIU Yuan[1], SHEN Xiaoyan[1], ZHOU Shinan[1], GUO Xubo[2], YU Jing[1], LI Dongsheng[1], LAN Xuhui[1]
(1 *College of Metrology & Measurement Engineering, China Jiliang University, Hangzhou* 310018, *China*)
(2 *Department of Physics, Tsinghua University, Beijing* 100084, *China*)

Abstract: A micro-angle measurement method based on Fabry-Perot etalon is proposed. Particularly, by calculating the displacement of center of the imaging concentric rings and the focal length of the imaging objective lens, the micro angle of the deflected mirror is obtained. The evaluation model of the micro angle uncertainty, based on the uncertainty components of the center displacement and the focal length of the imaging objective lens, is constructed. The Fabry-Perot etalon with an interval of 2 mm is selected to carry out the experimental research on the measurement of micro angles, and the data is processed. The experimental results indicate that the maximum measurement uncertainty is 0.132" and 0.045" in the range of 600" and 40", respectively. The proposed method can provide a reference for the realization of the self-calibrated, higher-accuracy micro-angle measurement.

Key words: Micro-angle measurement; Fabry-Perot etalon; High accuracy; Uncertainty analysis;

Foundation item: The National Natural Science Foundation of China (Nos. 51875543, 61605193), the Fundamental Research Funds for the Provincial Universities of Zhejiang (No. 2020YW03)

First author: LIU Yuan (1996—), male, M.S. degree candidate, mainly focuses on precision optical inspection technology and application. Email: ly3433@qq.com
Supervisor (Contact author): SHEN Xiaoyan (1982—), female, associate professor, Ph. D. degree, mainly focuses on the research of optical inspection and precision testing technology. Email: xyshen@cjlu.edu.cn

Received: Nov.17, 2020; **Accepted**: Jan.11, 2021

Measurement method
OCIS Codes: 120.2230; 120.3930; 120.3180

0 Introduction

Micro-angle measurement technology is widely utilized in the installation of precision mechanical components, precision and ultraprecision machining, as well as aiming and positioning. it is extremely important in the fields of machinery, aerospace, military, and other applications[1]. The photoelectric autocollimator is currently the main technical means to measure micro angles with high precision. It applies the optical autocollimation method to project the deflection angle of the incident light onto the image plane, and the displacement of the light spot is analyzed by the two-dimensional imaging device to measure the deflection angle. The world's leading manufacturers of photoelectric autocollimators are the UK (Taylor Hobson), Germany (MÖLLER-WEDEL), USA (API), and Japan (Nikon). The German ELCOMAT HR photoelectric autocollimation goniometer exhibits the highest precision. Its accuracy can reach 0.02", 0.04", and 0.06" in the range of 10", 40", and 300", respectively. Several studies on high-accuracy micro-angle measurement and related technologies have been conducted. In 2012, TANFER Y et al.[2] developed a high-precision micro-angle generator, which can be calibrated for photoelectric autocollimators, with an expanded uncertainty of 0.01" (coverage factor k=2). In 2013, KIM J A et al.[3] proposed a method for correcting the nonlinear error of the segmented circular periodic signal and achieved an uncertainty of less than 0.015". In 2016, HSIEH M C et al. [4] proposed a new optical material and a heterodyne interferometer for micro-angle measurement. In a dynamic range of 0.45°, the angle measurement resolution can be better than 0.252". In 2017, HEIKKINEN V et al.[5] studied a new type of interferometric two-way micro-angle generator with a standard uncertainty of 0.003 6" in the range of 2 000". Although China's angle measurement technology started late, it has achieved promising results. The AUTOMAT5000 photoelectric autocollimator produced by Tianjin Automate Optoelectronics Co., Ltd. has an accuracy of 0.25" and 0.1" in the range of 1 000" and 100", respectively. Its indicators are deemed domestic and of highest value among commercial products. In 2008, the 6 354 Research Institute of China State Shipbuilding Corporation [6] developed a high-precision dual-axis autocollimator with an accuracy of 0.2" in the range of 500″. The EAMP300 autocollimator developed by Beijing Aerospace Metrology and Testing Technology Research Institute in 2019[7] has an accuracy of 0.25" in the range of 1 000". In terms of angle measurement technology, ZHANG Junjie et al.[8] added the magnifying optical path to the optical path of the collimator to amplify the self-collimated image and its displacement and achieved an indication error of ±0.01" and ±0.02" in the range of 10" and 50", respectively. TAN Xinran et al.[9] proposed a micro-angle measurement method based on capacitive sensors, which achieved an accuracy of 0.157" and 0.052" in the range of 900" and 300", respectively. In 2018, WU Yumin et al.[10] proposed a micro-angle measurement method based on a lensless digital holographic microscope with an accuracy of 0.5" in the range of 1 000". In 2019, HE Yun et al.[11] studied a noncontact external right-angle measurement method; its accuracy was better than 0.1" and 0.4" in the range of 3.0" and 8.0", respectively. Obviously, there is still a significant gap in the research and development of domestic micro-angle products between countries.

This paper innovatively proposes a micro-angle measurement method based on Fabry-Perot (F-P) etalon. By calculating the displacement of the centers of the imaging concentric rings and the focal length of the imaging objective lens, a self-calibrating micro-angle measurement with high accuracy was realized. Moreover, an evaluation model of the uncertainty of micro-angle measurement was established.

1 Micro-angle measurement principle based on F-P etalon

The micro-angle measurement optical path based on F-P etalon is shown in Fig.1. The point light source passes through the interference filter to produce quasi-monochromatic light with a known vacuum wavelength λ_0, which, in turn, passes through the condenser lens to form a high-intensity extended light source, and subsequently passes through the F-P etalon with the clearance of d and a refractive index of n. After tooling, a series of standard cone beams with cone angle θ_i are produced. The conical beam passes through the reflected mirror and the imaging objective lens and forms several Concentric Interference Rings (CIRs) with a diameter

of D_i on the area array device at the focal plane. The conical beam passes through the reflected mirror and the imaging objective lens, forming several CIRs on the area array device at the focal plane. θ_i is the series cone angle between the conical beam and the conical axis perpendicular to the exit surface of the etalon. i is the serial number of the CIR. The first circle from the center is marked as $i=0, 1, 2, \cdots$. k_0 is the integer part of the smallest interference order of $\theta_i(i=0)$; the interference order is

$$k_0+\varepsilon=2dn/\lambda_0 \tag{1}$$

where ε is the fractional part of the interference order corresponding to k_0, with $0\leqslant\varepsilon<1$.

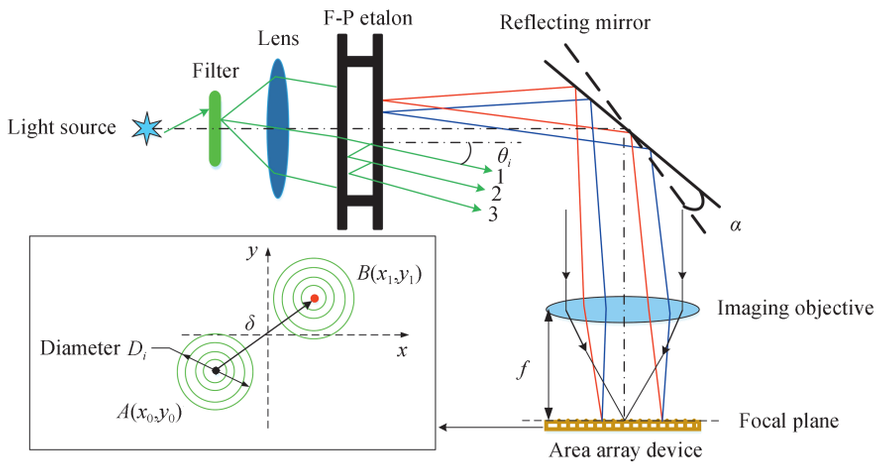

Fig. 1 Micro-angle measurement optical path based on F-P etalon

When the reflected mirror rotates through a micro angle α, the reflected beam tilts by 2α, and the position of the CIR on the rear array of the imaging objective corresponds to a micro center displacement δ. The coordinates of the center of the circle before and after the angular deflection are $A(x_0, y_0)$ and $B(x_1, y_1)$, respectively. Therefore, δ and its standard deviation are respectively

$$\delta_w=\delta/w=\sqrt{(x_1-x_0)^2+(y_1-y_0)^2} \tag{2}$$

$$s_{\delta_w}=\sqrt{\left(\frac{y_1-y_0}{\delta_w}\right)^2\times(s_{y_1}^2+s_{y_0}^2)+\left(\frac{x_1-x_0}{\delta_w}\right)^2\times(s_{x_1}^2+s_{x_0}^2)} \tag{3}$$

where $x_0, y_0, x_1, y_1, \delta_w$ are the average pixel coordinates with spacing w as the relative unit, and $s_{x_0}, s_{y_0}, s_{x_1}, s_{y_1}$ are the standard deviations of x_0, y_0, x_1, y_1. From the classical optical principle, the cone angle θ_i and the focal length f of the imaging objective lens determine the diameter D_i of the series of imaging concentric rings, and the specific relationship is[12]

$$\left(\frac{D_i/2}{f/w}\right)^2=(\tan\theta_i)^2=\left(\frac{k_0+\varepsilon}{k_0-i}\right)^2-1 \tag{4}$$

According to Eq. (1) and (4), the diameter D_i of the CIR and the corresponding ring number i are fitted with the least squares straight line, and the focal length of the imaging objective lens is

$$f_w=f/w\approx\frac{D_i}{2}\sqrt{\frac{k_0}{2(i+\varepsilon)}} \tag{5}$$

The relative expanded uncertainty of f_w is

$$\frac{U'_p(f_w)}{f_w}=t_p(v_{\text{eff}})\times\sqrt{\left(\frac{s_{f_w}}{f_w}\right)^2+\left(\frac{u_{\text{fad}}}{\sqrt{3}\,f_w}\right)^2+\left(\frac{u_w}{\sqrt{3}\,w}\right)^2} \tag{6}$$

where f_w is the average pixel interval w as the relative unit, $t_p(v_{\text{eff}})$ is the expansion factor obtained under the confidence probability p and effective degrees of freedomv_{eff}, s_{f_w} is the standard deviation of f_w, and u_{fad} is the uncertainty introduced by the focus error limit of the area array acquisition device. u_w is the uncertainty

component introduced by the average pixel pitch. According to the principle of geometric optics, f_w, δ_w, and α of the reflected mirror are related as $\delta_w = f_w \tan(2\alpha)$. To realize the α self-calibration feature and reduce the measurement error as much as possible, the average pixel spacing w is regarded as the relative unit, and the micro-angle calculation equation using the relative measurement principle is

$$\alpha = \frac{1}{2}\arctan\frac{\delta_w}{f_w} \tag{7}$$

The accurate measurement of f_w and δ_w is the key to the measurement of α. The research group has initially completed the related research on the measurement of f_w and δ_w[13-14]. Fig. 2 shows the basic process for measuring f_w and δ_w.

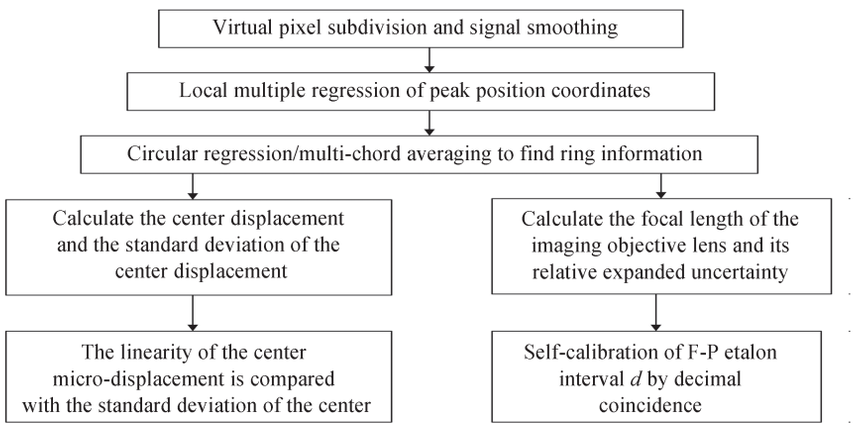

Fig. 2 Basic process of lens focal length and center micro-displacement measurement

First, perform virtual pixel subdivision and signal smoothing on the collected CIR image. The subdivided virtual pixel spacing is reduced to the original spacing $1/\sqrt{2}$. After smoothing, the influence of stochastic undetermined system error is reduced. Afterwards, the local multiple regression of peak position coordinates is performed to reduce the influence of pixel geometric error and photoelectric conversion rate error caused by various factors. Finally, the circular regression and multi-chord averaging method are used to obtain the ring information. From the ring information, the coordinates of the center of the circle and its standard deviation as well as the diameter of the ring and its standard deviation can be calculated. We calculate δ_w and s_{δ_w} from Eq. (2) and (3) and compare with the laser phase modulation differential interferometer to verify that the measurement of s_{δ_w} can reach submicron level. The focal value of the imaging objective lens and the value of $\frac{U'_p(f_w)}{f_w}$ are calculated by Eq. (5) and (6), respectively. Implementing the decimal repetition method[15] to measure the F-P etalon with the clearance of d accurately, we obtain the CIR information generated by the three different wavelengths after passing through the F-P etalon, calculate the ring diameter by circular regression, and apply mathematical statistics to calculate εand find d. The self-calibration of the α measurement can be realized.

2 Establishment and analysis of uncertainty evaluation model of micro-angle measurement

2.1 Uncertainty evaluation model of micro-angle measurement

Usually, $|\alpha| < 0.05\ \text{rad} \approx 2.86°$, from Eq. (7), it can be obtained that

$$\alpha \approx \frac{1}{2}\frac{\delta_w}{f_w} \tag{8}$$

According to Eq. (8), utilizing the indirect measurement method[16], the deflection α of the relative change of the ring center's δ_w is

$$\frac{\partial\alpha}{\partial\delta_w} = \frac{1}{2f_w} \tag{9}$$

The deviation of the deflection $\alpha$to f_w is calculated as

$$\frac{\partial \alpha}{\partial f_w} = -\frac{1}{2}\frac{\delta_w}{{f_w}^2} \tag{10}$$

Owing to the existence of $\sqrt{s_1^2+s_2^2} < s_1+s_2$ when the independent component standard deviation is synthesized, the standard deviation of (x_1-x_0) and (y_1-y_0) is $\sqrt{s_{x_0}^2+s_{x_1}^2+s_{y_0}^2+s_{y_1}^2} \approx \sqrt{4s_{x_0}^2} = \sqrt{2}\, s_{x_0}$. After a slight magnification, the expanded uncertainty $U_p(\alpha)$ of α can be written as

$$\begin{aligned} U_p(\alpha) \approx c_0 + c_1 \cdot |\alpha| = k_p \times \left(\frac{\partial \alpha}{\partial \delta_w}\sqrt{2}\, s_{x_0}\right) + k_p \times \left(\frac{\partial \alpha}{\partial f_w} s_{f_w}\right) = t_p(v) \times \left(\frac{\partial \alpha}{\partial \delta_w}\sqrt{2}\, s_{x_0}\right) + \\ t_p(v_{\text{eff}'}) \times \left(\frac{\partial \alpha}{\partial f_w} s_{f_w}\right) = t_p(v) \times \frac{\sqrt{2}\, s_{x_0}}{2f_w} + \left(t_p(v_{\text{eff}'}) \times \frac{s_{f_w}}{f_w}\right) \cdot |\alpha| \end{aligned} \tag{11}$$

where t is the distribution factor and v is the degree of freedom when seeking s_{x_0}, s_{x_0} can be obtained when applying the multiple regression mathematical statistics method to derive the position x_0 of the ring point, and v_{eff} is the effective degree of freedom[17].

According to Eq. (11), the measurement uncertainty of the rotation α is

$$\begin{aligned} U_p(\alpha) \approx c_0 + c_1 \cdot |\alpha| = k_p \times \frac{u_c(\delta_w)}{2f_w} + k_p \times \frac{u_c(f_w)}{f_w} \cdot |\alpha| = \\ t_p(v_{\text{eff1}}) \times \frac{u_c(\delta_w)}{2f_w} + t_p(v_{\text{eff2}}) \times \frac{u_c(f_w)}{f_w} \cdot |\alpha| \end{aligned} \tag{12}$$

where the sum component c_0 is related to the synthetic standard uncertainty $u_c(\delta_w)$ of δ_w and f_w, the magnification component c_1 is related to the synthetic standard uncertainty $u_c(f_w)$ of f_w. v_{eff1} is the effective degree of freedom of δ_w to the uncertainty of the synthetic standard, and v_{eff2} is the effective degree of freedom of f_w to the uncertainty of the synthetic standard. According to the Ref.[12], the effective resolution of the rotation α is $R_e(\alpha) \approx 0.2c_0$.

2.2 Expanded uncertainty of center displacement

The expanded uncertainty of δ_w is $U_p(\delta_w) = t_p(v_{\text{eff1}}) \times u_c(\delta_w)$. $u_c(\delta_w)$ mainly includes the uncertainty component $u_{1\,\text{rel}}$ introduced by the repeatability standard deviation of the circle center coordinate, the uncertainty component $u_{2\,\text{rel}}$ introduced by the deviation of the area array device from the focal plane, the uncertainty introduced by the idle distance error in the measurement system, and the certainty component $u_{3\,\text{rel}}$ and the uncertainty component $u_{4\,\text{rel}}$ introduced by the ambient temperature gradient distribution. Since the influencing variables are independent and uncorrelated, the expanded uncertainty expression of δ_w is

$$U_p(\delta_w) = k_p \times u_c(\delta_w) = t_p(v_{\text{eff1}}) \times u_c(\delta_w) = t_p(v_{\text{eff1}}) \times \sqrt{{u_{1\,\text{rel}}}^2 + {u_{2\,\text{rel}}}^2 + {u_{3\,\text{rel}}}^2 + {u_{4\,\text{rel}}}^2} \tag{13}$$

$$v_{\text{eff1}} = \frac{\left(\sqrt{{u_{1\,\text{rel}}}^2 + {u_{2\,\text{rel}}}^2 + {u_{3\,\text{rel}}}^2 + {u_{4\,\text{rel}}}^2}\right)^4}{\frac{{u_{1\,\text{rel}}}^4}{v_1} + \frac{{u_{2\,\text{rel}}}^4}{v_2} + \frac{{u_{3\,\text{rel}}}^4}{v_3} + \frac{{u_{4\,\text{rel}}}^4}{v_4}} \tag{14}$$

where v_1, v_2, v_3, v_4 are the corresponding degrees of freedom of $u_{1\,\text{rel}}, u_{2\,\text{rel}}, u_{3\,\text{rel}}, u_{4\,\text{rel}}$, respectively.

1) In the same experiment, the arithmetic mean of the standard deviation of δ_w corresponding to all α values is taken as the repeatability standard deviation $u_{1\,\text{rel}} = \bar{s}_{\delta_w}$ of the center coordinate.

2) When there is an angle between the area array device and the focal plane position, the interference image received by the area array device changes, causing the ring to be elliptical and affecting the accuracy of the center measurement. We suppose that the deflection center offset L of the area array device occurs and calculate the uncertainty component $u_{2\,\text{rel}} = \frac{L}{\sqrt{3}}$ according to the uniform distribution.

3) Idle distance error refers to the change of the optical path of the beam in the F-P etalon owing to changes in the external environment, which affects the measurement result. We define the idle time error $\Delta c = d\Delta n/\cos\theta$. Δn is the change value of the refractive index of the air before and after the environmental change. The F-P etalon with the clearance of d is calculated by the decimal repetition method; the uncertainty

component $u_{3\,\mathrm{rel}}=\dfrac{\Delta c}{\sqrt{3}}$ is calculated according to the uniform distribution.

4) The change of the environmental temperature gradient will cause the drift of the pixels to different positions of the area array. We define the amount $\Delta l=\beta l\Delta t$ of environmental gradient change, where β is the linear expansion coefficient of the area array substrate, l is the diameter of the ring involved in the calculation, and Δt is the temperature change. The uncertainty component $u_{4\,\mathrm{rel}}=\dfrac{\Delta l}{\sqrt{3}}$ is calculated according to the uniform distribution.

2.3 Expanded uncertainty of the focal length of the imaging objective lens

The expanded uncertainty $U_p(f_w)=t_p(\upsilon_{\mathrm{eff2}})\times u_c(f_w)$ of f_w and $u_c(f_w)$ mainly includes the uncertainty component $u_{5\,\mathrm{rel}}$ introduced by the measurement repeatability standard deviation of f_w and the uncertainty component $u_{6\,\mathrm{rel}}$ introduced by the focus error limit. Since the influence quantities are independent and unrelated, the expanded uncertainty expression of f_w is

$$U_p(f_w)=k_p\times u_c(f_w)=t_p(\upsilon_{\mathrm{eff2}})\times u_c(f_w)=t_p(\upsilon_{\mathrm{eff2}})\times\sqrt{{u_{5\,\mathrm{rel}}}^2+{u_{6\,\mathrm{rel}}}^2} \tag{15}$$

$$\upsilon_{\mathrm{eff2}}=\frac{\left(\sqrt{{u_{5\,\mathrm{rel}}}^2+{u_{6\,\mathrm{rel}}}^2}\right)^4}{\dfrac{{u_{5\,\mathrm{rel}}}^4}{\upsilon_5}+\dfrac{{u_{6\,\mathrm{rel}}}^4}{\upsilon_6}} \tag{16}$$

Among them, υ_5 and υ_6 are the degrees of freedom corresponding to $u_{5\,\mathrm{rel}}$ and $u_{6\,\mathrm{rel}}$, respectively.

1) The standard deviation of f_w is s_{f_w}, therefore, $u_{5\,\mathrm{rel}}=s_{f_w}$.

2) If the area array device cannot be accurately located before and after the focal plane, the image collected by the area array device is not the clearest. According to the Ref.[13], before the measurement of α, the focus experiment is carried out, the half maximum value of the shooting circle is calculated, and the focus error limit u_{fad} is determined after regression fitting. Hence, $u_{6\,\mathrm{rel}}=\dfrac{u_{\mathrm{fad}}}{\sqrt{3}}$.

3 Micro-angle measurement experiment

3.1 Experimental device and interference image acquisition

The measuring device of α is shown in Fig.3. The pen-shaped low-pressure mercury lamp as well as the mercury lamp light source are placed on the universal adjusting bracket. The light emitted by the light source passes through the interference filter to form a quasi-monochromatic light, which, in turn, is transmitted through the condensing lens, making the light source an expanded light source with higher intensity. The multi-directional incident light in a certain solid angle range from the expanded light source is transmitted through the F-P etalon to produce a standard coaxial conical beam, which passes through the reflected mirror and the industrial fixed focus lens successively to form a CIR. The center wavelength of the interference filter is about 546 nm, and the F-P etalon with the clearance of $d\approx 2$ mm. α is generated by the angle rotating table on

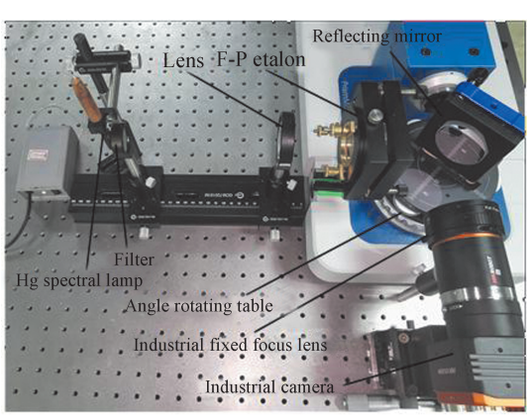

Fig. 3 Micro-angle measuring device

the PrismMaster® 150 MAN goniometer, the angle measurement accuracy is ±1.2". The flatness of the reflected mirror is better than $\lambda/20$. The measured objective lens model is HIKVISIONMVL-LF8040M-F 80 mm industrial fixed-focus lens, the camera adopts the HIKVISIONMV-CH430-90XM industrial camera, the area array size is 22.16 mm×15.22 mm, the area array pixel number is 7 904×5 432, and the average pixel spacing of the area array is $w \approx 2.8\ \mu m$.

After constructing the experimental device according to Fig.3, adjust the light path to be coaxial to ensure that the light intensity distribution that can be received on the area array device (industrial camera) is uniform. By adjusting the focus, we ensure that the best ring picture is rendered. When the angle rotating table produces a slight rotation (The angle rotating table only needs to produce an angle that meets the required range), α of the reflected mirror changes accordingly, and the position of the ring collected by the area array device (industrial camera) changes. Through the data processing of the images before and after the position of the ring changes, α is calculated. Fig.4 depicts a CIR with a wavelength of 546 nm rendered by an industrial camera. Fig.4 (a) shows the original CIR image, which is deployed for the subsequent calculation of f_w and center coordinates, and Fig.4 (b) shows the high-brightness CIR image, which is convenient for observation.

(a) Original CIR image (b) High brightness CIR image

Fig. 4 Concentric interference ring at 546 nm wavelength

3.2 CIR image quality and optimal ring selection

First, we judge the image quality of CIRs. The clarity of CIR and the degree of ring ellipse directly affect the subsequent data processing calculation. The Full Width at Half Maximum (FWHM) of the ring represents the phase difference when the photoelectric signal is half the maximum value. By adjusting the focus ring of the camera lens and calculating the FWHM of the ring, the best focus position is found, and the image is positioned onto the focal plane, making the ring clearest. Table 1 shows the FWHM values and their average values of CIR in the four directions of $x+$, $x-$, $y+$, $y-$ under different focusing positions $\overline{\text{FWHM}}$.

Table 1 FWHM value under different focusing positions (w)

Position	FWHM $x+$	FWHM $x-$	FWHM $y+$	FWHM $y-$	$\overline{\text{FWHM}}$
0	10.225	8.843	11.422	18.467	12.239
1	8.945	7.625	11.026	11.681	9.819
2	7.687	7.538	10.428	11.729	9.345
3	6.495	6.451	8.129	13.581	8.664
4	5.607	6.080	6.625	8.668	6.745
5	5.268	6.257	5.823	5.493	5.710
6	**5.356**	**6.001**	**6.052**	**5.316**	**5.681**
7	6.816	6.553	8.530	7.064	7.241
8	7.682	6.866	11.664	11.038	9.313
9	9.788	7.517	13.704	13.164	11.043
10	8.785	8.459	20.348	12.068	12.415

From Table 1, it is obvious that at focus position 6, the average FWHM is minimum and equals to $5.681w$. Therefore, since CIR is the clearest when captured at focusing position 6, that focusing position is selected as the best one. By further comparing the closeness of the FWHM values in the four directions at the

optimal focusing position, the size of the installation position error of the optical components can be judged, such as the angle between the area array device and the focal plane, and the measurement optical path is not coaxial.

Second, the best ring is selected. In the data processing of α measurement, when using the multi-chord averaging method to calculate the ring information, the optimal ring must be selected. According to the CIR data processing method from the Ref.[14], as shown in Fig. 5, the virtual pixel subdivision and signal smoothing are performed first, and the x axis and y axis are established in the horizontal and vertical directions of the approximate CIR diameter, respectively. We rotate the Cartesian coordinate system 45° counterclockwise to obtain the x', y' coordinate system, and perform interpolation and signal smoothing. We establish N parallel lines on both sides of the approximate circle diameter of the x', y' axis coordinate system; N is a positive integer. For the same ring, there will be $8N+4$ small line segments after the parallel line intersects each ring. The local multiple regression method is applied to obtain the accurate peak coordinate value and peak coordinate standard deviations. By calculating the mean value $\bar{s}$ of the standard deviation of the respective peak position coordinates of all the circles, the optimal circle is determined. As shown in Table 2, the minimum mean value of the standard deviation of the peak coordinates of the 12th ring is $0.015w'$ (w' is the pixel interval after the virtual pixel subdivision and signal smoothing). Therefore, the 12th ring is selected as the optimal ring, and the peak position coordinates on the optimal ring are deployed to calculate δ_w and f_w, and finally an α value with high accuracy is obtained.

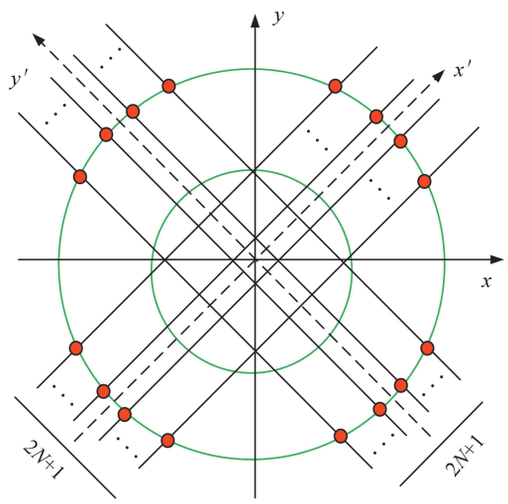

Fig. 5 Schematic diagram of circle data processing

Table 2 Calculated result of the standard deviations of the peak position coordinates in different directions and the average $\bar{s}(w')$

Serial number of the ring i	$s_{x'+}$	$s_{x'-}$	$s_{y'+}$	$s_{y'-}$	$\bar{s}$
1	0.080	0.088	0.081	0.090	0.085
2	0.056	0.064	0.056	0.064	0.060
3	0.043	0.061	0.052	0.056	0.053
4	0.034	0.052	0.043	0.047	0.044
5	0.033	0.046	0.041	0.038	0.039
6	0.024	0.044	0.038	0.035	0.035
7	0.019	0.046	0.031	0.027	0.031
8	0.016	0.039	0.026	0.024	0.026
9	0.017	0.030	0.023	0.019	0.022
10	0.015	0.033	0.015	0.013	0.019
11	0.015	0.029	0.013	0.012	0.017
12	**0.015**	**0.025**	**0.012**	**0.010**	**0.015**
13	0.018	0.021	0.012	0.011	0.016
14	0.019	0.023	0.015	0.011	0.017
15	0.019	0.019	0.014	0.014	0.017
16	0.021	0.016	0.014	0.014	0.016
17	0.025	0.017	0.017	0.014	0.018

3.3 CIR image quality and optimal ring selection

According to the imaging position of the CIR on the area array device, a certain number of rings can be collected when the angle rotating table rotates in 600". Because of the α measurement, the measured value of the f_w of the industrial fixed focus lens is stable in a certain range, the CIR shot at the initial position of the angle rotation stage is exploited to calculate f_w. In the experiment, the temperature is 24.6 ℃ and the humidity is 65%. Along the same direction, we rotate once every 100" interval and take one shot every 1 min before each rotation. A total of three shots are taken to verify the repeatability of the measurement and complete the 600" measurement experiment. As shown in Table 3, according to the shooting time, the α position and the number of times are marked with the serial number. For example, the serial number of the first shot at position 0 is marked as 0-1. For the sake of convenience, the unit of the measured f has been converted to millimeters, δ and s_δ are converted to micrometers, and the measured f is evaluated using $\frac{U'_p(f_w)}{f_w}$.

Table 3 Experimental results of 600″ inner angle measurement

No.	f/mm	$\frac{U'_p(f_w)}{f_w}$	δ/μm	s_δ/μm	α/(″)	$U_p(\alpha)_1$/(″)
0-1			0.157	0.012	0.207	0.041
0-2			0.269	0.012	0.354	0.041
0-3			0.263	0.012	0.348	0.041
1-1			76.991	0.014	101.567	0.056
1-2			77.169	0.013	101.802	0.056
1-3			77.237	0.012	101.891	0.056
2-1			153.655	0.014	202.701	0.071
2-2			153.699	0.013	202.759	0.071
2-3			153.806	0.013	202.900	0.071
3-1			230.224	0.012	303.710	0.087
3-2	78.18	0.014	230.291	0.012	303.800	0.087
3-3			230.434	0.013	303.988	0.087
4-1			306.901	0.012	404.863	0.102
4-2			306.958	0.012	404.937	0.102
4-3			307.099	0.011	405.123	0.102
5-1			383.563	0.012	505.993	0.117
5-2			383.611	0.012	506.057	0.117
5-3			383.819	0.012	506.330	0.117
6-1			460.229	0.012	607.128	0.132
6-2			460.323	0.012	607.252	0.132
6-3			460.297	0.012	607.217	0.132

According to the measurement principle of CIR pictures before and after the α rotation (Section 1), f_w, $\frac{U'_p(f_w)}{f_w}$, δ_w, and s_{δ_w} are calculated. α is calculated by Eq. (7). According to the α measurement uncertainty evaluation model (Section 2.1), the α measurement uncertainty $U_p(\alpha)_1 = 0.041'' + 1.5 \times 10^{-4} \cdot |\alpha|$ is calculated by Eq. (12), and the effective resolution $R_{e1}(\alpha) \approx 0.2c_0 \approx 0.008''$ of the rotation α is calculated. Table 4 shows the calculation of measurement uncertainty.

The experimental results indicate that f is 78.178 mm, $\frac{U'_p(f_w)}{f_w}$ is 0.014, and s_δ is not more than 14 nm in the range of 600″. The α measurement uncertainty is less than 0.132″ and has good repeatability.

Table 4 Calculation instructions of measurement uncertainty $U_p(\alpha)_1$

Measurement uncertainty	Uncertainty component	Expression
$U_p(\delta_w)$ ($\upsilon_{\text{eff1}}=39, p=0.95$)	$u_{1\,\text{rel}}$	Take 15th s_{δ_w}, $u_{1\,\text{rel}}=\bar{s}_{\delta_w}=0.0030w'$
	$u_{2\,\text{rel}}$	$L\leqslant\pm0.001w', u_{2\,\text{rel}}=\dfrac{L}{\sqrt{3}}=5.8\times10^{-4}w'$
	$u_{3\,\text{rel}}$	d=2015522.7 nm, $\Delta n=\pm4.75\times10^{-7}$, Cosine of the cone angle of the optimal ring $\cos\theta=0.9983$, $u_{3\,\text{rel}}=\dfrac{\Delta c}{\sqrt{3}}=\dfrac{d\Delta n/\cos\theta}{\sqrt{3}}=1.4\times10^{-4}w'$
	$u_{4\,\text{rel}}$	$\beta=3.5\times10^{-6}K^{-1}$, Optimal ring diameter $l=2328.978w'$, $\Delta t\leqslant\pm0.5$℃, $u_{4\,\text{rel}}=\dfrac{\Delta l}{\sqrt{3}}=\dfrac{\beta l\Delta t}{\sqrt{3}}=0.0024w'$
$U_p(f_w)$ ($\upsilon_{\text{eff2}}=21, p=0.95$)	$u_{5\,\text{rel}}$	$f_w=19743.904w', s_{f_w}=0.13w', u_{5\,\text{rel}}=s_{f_w}=0.13w'$
	$u_{6\,\text{rel}}$	$u_{\text{fad}}=\pm2.466w', u_{6\,\text{rel}}=\dfrac{u_{\text{fad}}}{\sqrt{3}}=1.4w'$

3.4 Experimental results and analysis of 40" internal angle measurement

According to the imaging position of the CIR on the area array device, a certain number of rings can be collected when the angle rotating table rotates in the range of 40″. Because of the measurement, the measured value of the industrial fixed focus lens is stable in a certain range, the CIR shot at the initial position of the angle rotation stage is implemented to calculate f_w. In the experiment, the temperature is 24.6℃ and the humidity is 65%. Along the same direction, we rotate once every 10″ interval and take one shot every 1 min before each rotation. A total of three shots are taken to verify the repeatability of the measurement and complete the 40″ measurement experiment. As shown in Table 4, according to the shooting time, the α position and the number of times are marked with the serial number. For example, the serial number of the first shot at position 0 is marked as 0-1. For the sake of convenience, the unit of the measured f has been converted to millimeters, δ and s_δ are converted to micrometers, and the measured f is evaluated using $\dfrac{U'_p(f_w)}{f_w}$.

According to the measurement principle of the CIR pictures before and after the α rotation (Section 1), f_w, $\dfrac{U'_p(f_w)}{f_w}$, δ_w, and s_{δ_w} are calculated. α is calculated by Eq. (7). According to the α measurement uncertainty evaluation model (Section 2), the α measurement uncertainty $U_p(\alpha)_2=0.038''+1.6\times10^{-4}\cdot|\alpha|$ is calculated by Eq. (15), and the effective resolution $R_{e2}(\alpha)\approx0.2c_0\approx0.008''$ of the rotation α is calculated. Table 5 shows

Table 5 Experimental results of 40″ inner angle measurement

No.	f/mm	$\dfrac{U'_p(f_w)}{f_w}$	δ/μm	s_δ/μm	α/(″)	$U_p(\alpha)_2$/(″)
0-1			0.163	0.010	0.216	0.038
0-2			0.162	0.011	0.214	0.038
0-3			0.138	0.012	0.181	0.038
1-1			7.630	0.012	10.069	0.040
1-2			7.676	0.011	10.129	0.040
1-3			7.550	0.011	9.962	0.040
2-1			15.770	0.011	20.810	0.041
2-2	78.157	0.014	15.912	0.011	20.996	0.041
2-3			15.939	0.011	21.032	0.041
3-1			24.089	0.012	31.786	0.043
3-2			24.176	0.011	31.901	0.043
3-3			24.181	0.012	31.908	0.043
4-1			32.446	0.012	42.814	0.045
4-2			32.602	0.012	43.020	0.045
4-3			32.516	0.012	42.906	0.045

the calculation of measurement uncertainty. The experimental results show that f is 78.157 mm, $\frac{U'_p(f_w)}{f_w}$ is 0.014, and s_δ is not more than 12 nm. The α measurement uncertainty is less than 0.045″ and has good repeatability.

4 Conclusion

In this paper, we introduced the α measurement principle based on F-P etalon multi-beam imaging, built its measurement uncertainty evaluation model, and specifically analyzed the uncertainty components introduced by the measurement of δ and f. Furthermore, we completed the establishment of an α measurement experimental device, studied the judgment of the image quality of the CIR and the selection of the optimal ring, and measured δ and f through the data processing of CIR image. Our aim was to attain a high-accuracy measurement of α. The results indicated that the α measurement uncertainty in the range of 600″ and 40″ was lower than 0.132″ and 0.045″, respectively. Moreover, our method has the advantages of simple structure, large measuring range, high accuracy, and self-calibration.

From Eq. (12), it is apparent that the additive component and magnification component of the measurement uncertainty of the α decreased with the increase in f. When the imaging objective lens with f=300 mm and the large area array were employed, the measurement uncertainty of α was reduced to about a quarter of the existing one, and could be expressed as $U_p(\alpha)=0.010''+3.8\times10^{-5}\cdot|\alpha|$. Therefore, the measurement uncertainty in the range of 600″ and 40″ could be less than 0.033″ and 0.012″, respectively. In terms of measurement accuracy and range, our method had better results than ELCOMAT HR photoelectric autocollimation goniometer.

References

[1] ZHONG Jingang, ZHANG Xianhua, JU Zhixiang. Absolute small-angle measurement based on optical feedback interferometry[J]. Chinese Optics Letters, 2008, 6(11): 830-832.

[2] TANFER Y, BULENT O, NURAY K. High precision small angle generator for realization of the SI unit of plane angle and calibration of high precision autocollimators[J]. Measurement Science and Technology, 2012, 23(9): 094006.

[3] KIM J A, KIM J W, KANG C S, et al.Calibration of angle artifacts and instruments using a high precision angle generator [J]. International Journal of Precision Engineering & Manufacturing, 2013, 14(3): 367-371.

[4] HSIEH M C, LIN J Y , CHEN Y F, et al. Measurement of small angle based on a (100) silicon wafer and heterodyne interferometer[J]. Optical Review, 2016, 23(3): 487-491.

[5] HEIKKINEN V, BYMAN V, PALOSUO I, et al. Interferometric 2D small angle generator for autocollimator calibration [J].Metrologia, 2017, 54(3):253-261.

[6] GAN Junhong, ZOU Jiugui, JI Guoding. Application of area array CCD in dual-axis autocollimator[J]. Infrared and Laser Engineering,2008,37(S1):60-62.

[7] Beijing Institute of Aerospace Metrology and Testing Technology[EB/OL]. [2020-11-17]. https://kns.cnki.net/kcms/detail/detail.aspx?dbcode=CJFD&dbname=CJFDLAST2019&filename=HWYJ201904001&v=3Aa8rYle1V41qgvz9Eeqfi%25mmd2BL5pZINk85bQ2GRCa3yXfv9urdNuDxBq3%25mmd2Fnvbg8SOq.

[8] ZHANG Junjie, LI Zhengyang, YE Shenghua. Adopting optical amplification to improve the resolution of photoelectric autocollimator[J]. Chinese Journal of Sensors and Actuators,2011,24(1):50-52.

[9] TAN Xinran, ZHU Fan, WANG Chao, et al. Improved accuracy of capacitive sensor-based micro-angle measurement with angular-to-linear displacement conversion[J].Review of Scientific Instruments, 2017, 88(11): 115104.

[10] WU Yumin, CHENG Haobo, WEN Yongfu. High-precision rotation angle measurement method based on a lensless digital holographic microscope[J]. Applied Optics,2018,57(1) :112-118.

[11] HE Yun, LIU Qi, HE Jingjing, et al. External right-angle measurement using a two-autocollimator system[J]. Applied Optics, 2019, 58(4): 1158-1163.

[12] ZHU Henian, XIAO Zhigang, HOU Yufei, et al. A Fabry-Perot etalon method for measuring focal length and rotationangle: CN, 201510217472.7[P]. 2019-09-20.

[13] SHEN Xiaoyan, SUN Zhipeng, HU Jiacheng, et al. Method for measuring focal length of transmission objective lens based on F-P etalon [J]. Chinese Journal of Scientific Instrument, 2018, 39(5): 1-8.

[14] SHEN Xiaoyan, LAN Xuhui, ZHU Henian, et al. Submicron displacement measurement method based on Fabry-Perot etalon[J]. Chinese Journal of Lasers, 2019, 46(12): 1204002.

[15] LAN Xuhui, SHEN Xiaoyan, SUN Zhipeng, et al. Subdivision of area array pixels for Fabry-Perot etalon interval

measurement[J]. Journal of Applied Optics, 2019, 40(1): 99-104.
[16] ZHU Henian. Lecture on new concept basic physics experiment [M]. Beijing: Tsinghua University Press, 2013: 16-17.
[17] General Administration of Quality Supervision, Inspection and Quarantine of the People's Republic of China. JJF 1059.1-2012, The National Metrology Specifications of the People's Republic of China: Evaluation and Expression of Measurement Uncertainty[S]. Beijing: China Standards Press, 2013.